MACCA: Offline Multi-agent Reinforcement Learning with Causal Credit Assignment

Ziyan Wang *ziyan.wang@kcl.ac.uk*
King's College London

Yali Du *yali.du@kcl.ac.uk*
King's College London

Yudi Zhang *y.zhang5@tue.nl*
Eindhoven University of Technology

Meng Fang *meng.fang@liverpool.ac.uk*
University of Liverpool
Eindhoven University of Technology

Biwei Huang *bih007@ucsd.edu*
University of California San Diego

Reviewed on OpenReview: *https://openreview.net/forum?id=gwUOzI4DuV*

Abstract

Offline Multi-agent Reinforcement Learning (MARL) is valuable in scenarios where online interaction is impractical or risky. While independent learning in MARL offers flexibility and scalability, accurately assigning credit to individual agents in offline settings poses challenges because interactions with an environment are prohibited. In this paper, we propose a new framework, namely **M**ulti-**A**gent **C**ausal **C**redit **A**ssignment (**MACCA**), to address credit assignment in the offline MARL setting. Our approach, MACCA, characterizing the generative process as a Dynamic Bayesian Network, captures relationships between environmental variables, states, actions, and rewards. Estimating this model on offline data, MACCA can learn each agent's contribution by analyzing the causal relationship of their individual rewards, ensuring accurate and interpretable credit assignment. Additionally, the modularity of our approach allows it to integrate with various offline MARL methods seamlessly. Theoretically, we proved that under the setting of the offline dataset, the underlying causal structure and the function for generating the individual rewards of agents are identifiable, which laid the foundation for the correctness of our modeling. In our experiments, we demonstrate that MACCA not only outperforms state-of-the-art methods but also enhances performance when integrated with other backbones.

1 Introduction

Offline Reinforcement learning (RL) has gained significant popularity in recent years. It can be particularly valuable in situations where online interaction is impractical or infeasible, such as the high cost of data collection or the potential danger involved (Levine et al., 2020). In the multi-agent setting, offline multi-agent reinforcement learning (MARL) has identified and addressed some of the challenges inherited from offline single-agent RL, such as distributional shift and partial observability (Du et al., 2023). For example, ICQ (Yang et al., 2021) focuses on the vulnerability of multi-agent systems to extrapolation errors, and CQL (Kumar et al., 2020) aims to mitigate overestimation in Q-values, which can lead to suboptimal policy learning. The independent learning paradigm in MARL is appealing due to its flexibility and scalability, making it a promising approach to solving complex problems in dynamic environments. While independent learning in MARL has its merits, it will significantly hinder algorithm efficiency when the offline dataset

only includes team rewards. This presents a credit assignment problem, aiming to assign credit to individual agents within partial observability and emergent behavior. While plain reward regression methods directly map joint state-action pairs to a single scalar reward, they inherently lack interpretability, as they do not reveal which specific dimensions of states or actions drive each agent's individual contributions. In contrast, employing a causal model explicitly captures these critical dependencies, providing clarity on each agent's causal influence and enabling more effective and interpretable credit assignment.

In offline MARL, addressing the issue of credit assignment is challenging. Agents are reliant on static, pre-collected datasets, often spanning a variety of behavior policies and actions across different time periods. This diversity in data distributions increases the difficulty of assigning credits, given that the nuances of agent contributions are lost in the plethora of policies. Recent credit assignment methods, such as SQDDPG (Wang et al., 2020) and SHAQ (Wang et al., 2022a), are primarily conceived for online scenarios where continuous feedback aids in refining credit assignments. However, when restricted to static offline data in offline MARL, they miss out on the essential dynamism and agility needed to accurately understand the intricate interplay within the dataset. Moreover, in offline settings, methods like SHAQ, which rely on the Shapley value, and SQDDPG, which employs a Shapley-like approach for individual Q-value estimation, face inherent challenges. Computing the Shapley value or its approximations demands consideration of every potential agent coalition, a process that is computationally intensive. In offline MARL, such approximations can lead to imprecise credit assignments due to a loss in precision, potential data inconsistencies from the static nature of past interactions, and scalability issues, especially when numerous agents operate in intricate environments.

In this paper, we propose a new framework, namely **M**ulti-**A**gent **C**ausal **C**redit **A**ssignment (**MACCA**), to address credit assignment in an offline MARL setting. MACCA equates the importance of the credit assignment and how the agent makes the contribution by causal modeling. MACCA first models the generation of individual rewards and team reward from the causal perspective, and construct a graphical representation, as shown in Figure 1, over the involved environment variables, including all the dimensions of states and actions of all agents, the individual rewards and the team rewards. Our method treats team reward as the causal effect of all the individual rewards and provides a way to recover the underlying parametric model, supported by the theoretical evidence of identifiability. In this way, MACCA offers the ability to distinguish the credit of each agent and gain insights into how their states and actions contribute to the individual rewards and further to the team reward. This is achieved through a learned parameterized generative model that decomposes the team reward into individual rewards. The causal structure within the generative process further enhances our understanding by providing insights into the specific contributions of each agent. With the support of theoretical identifiability, we identify the unknown causal structure and individual reward function in such a causal generative process. Additionally, our method offers a clear explanation for actions and states leading to individual rewards, promoting policy optimization and invariance. This clarity enhances agent behavior comprehension and aids in refining policies. The inherent modularity of MACCA ensures its compatibility with a range of policy learning methods, positioning it as a versatile and promising MARL solution for various real-world contexts.

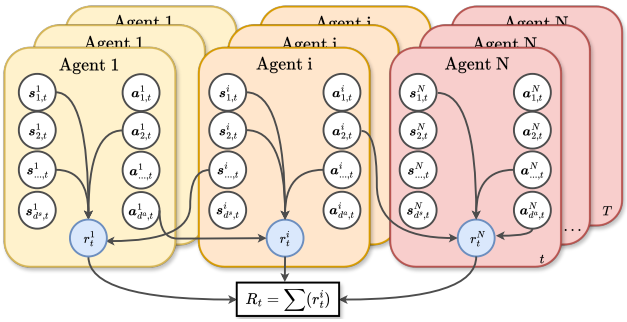

Figure 1: The graphic representation of the causal structure within the MACCA framework. The nodes and edges represent the causal relationships among various environmental variables, i.e., different dimensions of these variables for each agent within the team reward Multi-agent MDP context. These dimensions include the different dimensions of the state $s^i_{\dots,t}$, action $a^i_{\dots,t}$, individual reward r^i_t for agent i, and the team reward R_t. The individual reward r^i_t (shown with blue filling) is unobservable, and the aggregation of r^i_t equals R_t.

We summarize the main contributions of this paper as follows. First, we reformulate team reward decomposition by introducing a Dynamic Bayesian Network (DBN) to describe the causal relationship among states, actions, individual rewards, and team reward. We provide theoretical evidence of identifiability to learn the causal

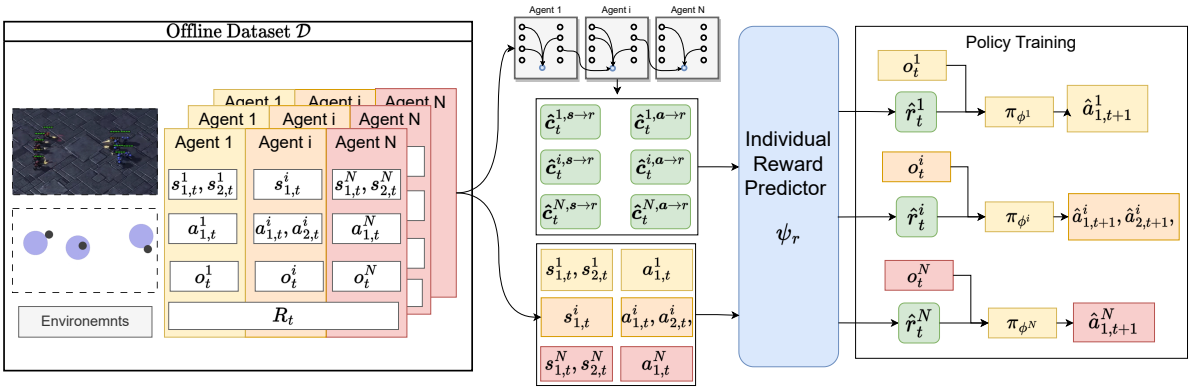

Figure 2: The illustration of the MACCA method. The offline data generation process begins on the left side, where data is recorded from the environment. MACCA then constructs a causal model consisting of a DBN represented in grey and an individual reward predictor depicted in blue. The DBN is used to sample scales from each agent, denoted as $c_t^{i,\cdot\to\cdot}$ and highlighted in green. Meanwhile, the individual reward predictor takes the joint state, action, and these masks as input to generate the individual reward estimate $\hat{r}_t^i$. During the policy learning phase, each agent utilizes their observation and individual reward estimate as inputs, which are then passed through their respective policy network to generate the next-state actions.

structure and function within the generation of individual rewards and team rewards. Second, our proposed method can recover the parameterized underlying generative process. Lastly, the empirical results on both discrete and continuous action settings, all three environments, demonstrate that MACCA outperforms current state-of-the-art methods in solving the credit assignment problem caused by team rewards.

2 Related Work

In this section, we review the close-related topics, *i.e.*, Offline MARL and Multi-agent Credit Assignment and Causal Reinforcement Learning.

Offline MARL. Recent research (Pan et al., 2022; Kostrikov et al., 2022; Jiang & Lu, 2021) efforts have delved into offline MARL, identified and addressed some of the issues inherited from offline single-agent RL (Agarwal et al., 2020; Yu et al., 2020; Yang et al., 2022; Wang et al., 2023). For instance, ICQ (Yang et al., 2021) focuses on the vulnerability of multi-agent systems to extrapolation errors, while MABCQ (Jiang & Lu, 2021) examines the problem of mismatched transition distributions in fully decentralized offline MARL. However, these studies all assume using a global state and evaluate the action of the agents relying on the team rewards. Other approaches (Tseng et al., 2022) have a long term progress in online fine-tuning for offline MARL training but have not taken into account the learning slowdown caused by credits of agents to the entire team. For the learning framework, the two most popular recent paradigms are Centralized Training with Decentralized Execution (CTDE) and Independent Learning (IL). Recent research (de Witt et al., 2020; Lyu et al., 2021) shows the benefits of decentralized paradigms, which lead to more robust performance compared to a centralized value function.

Multi-agent Credit Assignment. Multi-agent Credit Assignment is the study to decompose the team reward to each individual agent in the cooperative multi-agent environments (Chang et al., 2003; Du et al., 2019; Chen et al., 2023). Recent works (Sunehag et al., 2018; Foerster et al., 2018; Wang et al., 2020; Rashid et al., 2020; Li et al., 2021) focus on value function decompose under online MARL manner. For instance, COMA (Foerster et al., 2018) is a representative method that uses a centralized critic to estimate the counterfactual advantage of an agent action, which is an on-policy algorithm. This means it requires the corresponding data distribution and samples consistent with the current policy for updates. However, in an offline setting, agents are limited to previously collected data and can't interact with the environment. This data, often from varying behavioral policies, might not align with the current policy. Therefore, COMA cannot be directly extended to the offline setting without changing its on-policy features (Levine et al., 2020).

In online off-policy settings, state-of-the-art credit assignment algorithms such as SHAQ (Wang et al., 2022a) and SQDDPG (Wang et al., 2020) utilize an agent's approximate Shapley value for credit assignment. In the experiment section, we conduct a comparative analysis with these methods, and the results for MACCA demonstrate superior performance. Note that we focus on explicitly decomposing the team reward into individual rewards in an offline setting under the casual structure we learned, and these decomposed rewards will be used to reconstruct the offline dataset first and further the policy learning phase.

Causal Reinforcement Learning. Plenty of work explores solving diverse RL problems with causal structures. Most research emphasizes the transferability of RL agents. For instance, Huang et al. (2021) learn factored representations and domain-specific change factors, while Feng et al. (2022) extend these ideas to handle non-stationary environments. More recently, Wang et al. (2022b) and Pitis et al. (2022) propose removing unnecessary dependencies in causal dynamics models to enhance generalization to unseen states. Hu et al. (2023) exploit causal relationships between actions and reward components to reduce gradient variance during policy learning, and Zhang et al. (2023) leverage causal structures to solve single-agent temporal credit assignment problems. Additionally, causal modeling has been introduced into multi-agent tasks (Grimbly et al., 2021; Jaques et al., 2019), model-based RL (Zhang & Bareinboim, 2016), and imitation learning (Zhang et al., 2020). In the context of games, Hammond et al. (2023) extend Pearl's causal hierarchy (Pearl, 2009b) to game-theoretic scenarios, developing structural causal games to analyze causal effects and counterfactual reasoning among fully observable, rational agents. However, unlike these prior approaches, our method specifically addresses offline settings in partially observable Dec-POMDPs, requiring a causal-identifiability proof to reliably recover individual rewards and causal structures from static datasets. Thus, MACCA complements existing causal RL methods by uniquely targeting causal reward decomposition to facilitate decentralized policy learning under partial observability and offline constraints.

3 Preliminaries

In this section, we review the widely-used MARL training framework, the Decentralized Partially Observable Markov Decision Process, and briefly introduce Offline MARL.

Decentralized Partially Observable Markov Decision Process (Dec-POMDP) (Oliehoek et al., 2016) is defined by a tuple $\mathcal{M} = \langle N, \mathcal{S}, \mathcal{A}, \mathcal{P}, \mathcal{R}, \mathcal{O}, \gamma \rangle$. In this tuple, N represents the number of agents, $\mathcal{S}$ is the state space, and $\mathcal{A}$ is the shared action spaces and $a^i \in \mathcal{A}$ is the action for agent i. The state transition function $\mathcal{P}(s'|s, \boldsymbol{a})$ specifies the probability of transitioning to a new state given the current state s and joint actions $\boldsymbol{a} = (a^1, \ldots, a^N)$. The $R_t = \mathcal{R}(s, \boldsymbol{a})$ is the team reward given by the team reward function and $o^i = \mathcal{O}(s, i)$ is the local observation for agent i at global state s. Each agent use a policy $\pi_\theta(a^i|o^i)$ parameterized by θ to produce an action a^i from the local observation o^i, and optimize the discounted accumulated team reward $J_\pi = \mathbb{E}[\sum_{t=0}^{\infty} \gamma^t \mathcal{R}(s_t, \boldsymbol{a}_t)]$, where $\boldsymbol{a}_t = (a_t^1, \ldots, a_t^N)$ is the joint action at time step t, and γ represents the discount factor.

We assume that the observed team reward R_t can be expressed as the sum of individual rewards, i.e. $R_t = \sum_{i=1}^{N} r_t^i$. Although this does not hold for every cooperative task, it is exactly true (or nearly so) in many common benchmarks (e.g. MPE, SMAC). Importantly, as we will demonstrate later via ablation studies, MACCA remains effective even when the true reward is not strictly additive.

Offline MARL. Under offline setting, we consider a MARL scenario where agents sample from a fixed dataset $\mathcal{D} = \{s_t^i, o_t^i, a_t^i, R_t, s_t^{i'}, o_t^{i'}\}$. This dataset is generated from the behavior policy π_b without any interaction with the environments, meaning that the dataset is pre-collected offline. Here, s_t^i, o_t^i and a_t^i represent the state, observation and action of agent i at time t, while R_t is the team reward received at time t, and $s_t^{i'}$, $o_t^{i'}$ represents the next state and observation of agent i.

Dynamic Bayesian Networks (DBN) (Murphy, 2002) is a graphical model for representing the joint distribution over a sequence of random variables across time. A DBN consists of repeated "time slices," where each slice t contains a set of variables (e.g. X_t), and edges within the slice encode contemporaneous dependencies. Between slices, directed edges specify how variables at time t influence variables at time $t+1$,

typically under a first-order Markov assumption:

$$P(X_{1:T}) \;=\; P(X_1)\prod_{t=2}^{T} P\big(X_t \mid X_{t-1}\big).$$

Each conditional distribution $P(X_t \mid X_{t-1})$ further factorizes according to the intra-slice structure at time t. In this way, a DBN compactly encodes both temporal transitions and within-slice conditional independencies.

4 Offline MARL with Causal Credit Assignment

Credit assignment plays a crucial role in facilitating the effective learning of policies in offline cooperative scenarios. In offline MARL, effectively assigning credit among agents is inherently challenging due to partial observability and the static nature of the data. A traditional Decentralized Partially Observable Markov Decision Process (Dec-POMDP) implicitly captures temporal causality; however, it does not explicitly specify which exact dimensions of an agent's state or action affect its individual reward. A generic reward-prediction network—such as a standard regression from joint states and actions directly to a single scalar reward—cannot reveal which agent-specific state-action dimensions drive each agent's contributions, leading to limited interpretability and an absence of sparsity.

To overcome these limitations, we propose MACCA, a method leveraging a causal modeling approach. Specifically, MACCA introduces a Dynamic Bayesian Network (DBN)(Murphy, 2002) to explicitly characterize causal relationships among variables. By learning binary masks, MACCA clearly identifies which subsets of the joint state-action variables causally influence each agent's individual reward, ensuring interpretability and sparsity. Moreover, our DBN formulation guarantees the identifiability of the true causal structure and individual reward functions under standard assumptions—namely the faithfulness and Markov conditions (see Proposition4.1). These critical properties significantly enhance the effectiveness of spatial credit assignment, particularly in scenarios where individual agent rewards are unobservable and further interaction with the environment is impossible.

In the following sections, we first present the underlying generative process within the offline MARL scenario, which serves as the foundation of our method. Then, we describe how to recover the underlying generative process and perform policy learning with the assigned individual rewards.

As shown in Figure 2, our method includes two main components: a causal model ψ_{m} and a policy model ψ_π. The overall objective, denoted as L_{MACCA}, consists of two key terms: (1) a model estimation loss L_{m}, which measures how accurately the individual reward predictor reconstructs the observed team reward from predicted individual reward components, along with an ℓ_1 penalty to enforce sparsity in causal masks, and (2) an offline policy learning loss J_π, computed based on standard offline RL algorithms (such as CQL, OMAR, or ICQ), using the assigned individual rewards instead of the team reward. Thus, our combined loss function can be expressed as:

$$L_{\mathrm{MACCA}} = L_{\mathrm{m}} + J_\pi, \tag{1}$$

where the specific form of J_π depends on the offline RL algorithm used (e.g., J_π^{CQL}, J_π^{OMAR}, or J_π^{ICQ} in this paper).

4.1 Underlying Generative Process in MARL

As a foundation of our method, we introduce a Dynamic Bayesian Network (DBN) (Murphy, 2002) to characterize the underlying generative process. DBN is a special type of graphical model that captures the temporal dependencies between variables, corresponding to state transitions across time steps in sequential decision making. By leveraging the DBN structure, we can naturally account for the graph structure over state, action, and reward variables, as well as their temporal dependencies, leading to a natural interpretation of the explicit contribution of each dimension of state and action towards the individual rewards.

We denote the $\mathcal{G}$ as the DBN to represent the causal structure between the states, actions, individual rewards, and team reward as shown in Figure 1, which is constructed over a finite number of random variables as $(s^i_{1,t}, \cdots, s^i_{d^i_s,t}, a^i_{1,t}, \cdots, a^i_{d^i_a,t}, r^i_t, R_t)_{i,t=1}^{N,T}$, where the d^i_s and d^i_a correspond to the dimensions of the state and action of agent i respectively. R_t is the observed team reward at time step t. r^i_t is the unobserved individual

reward at time step t. T is the maximum episode length of the environment. Then, the underlying generative process is denoted as:

$$\begin{cases} r_t^i \;=\; f\big(\boldsymbol{c}^{i,\,\boldsymbol{s}\to r}\odot \boldsymbol{s}_t,\; \boldsymbol{c}^{i,\,\boldsymbol{a}\to r}\odot \boldsymbol{a}_t,\; i,\; \varepsilon_{i,t}\big), \\ R_t \;=\; \sum_{i=1}^{N} r_t^i, \end{cases} \tag{2}$$

where $\varepsilon_{i,t}$ denotes an exogenous noise term that is independent and identically distributed across agents and time—i.e. standard structural-causal-model noise—to account for variability beyond the deterministic mapping f. Here, $\boldsymbol{s}_t = \{s_{1,t}^1, \ldots, s_{d_s^1,t}^1, \ldots, s_{1,t}^N, \ldots, s_{d_s^N,t}^N\}$ and $\boldsymbol{a}_t = \{a_{1,t}^1, \ldots, a_{d_a^1,t}^1, \ldots, a_{1,t}^N, \ldots, a_{d_a^N,t}^N\}$ are the joint state and joint action of all N agents at time t, with $D_{\boldsymbol{s}} = \sum_{i=1}^N d_{\boldsymbol{s}}^i$ and $D_{\boldsymbol{a}} = \sum_{i=1}^N d_{\boldsymbol{a}}^i$ denoting their respective total dimensions. The operator $\odot$ is element-wise multiplication, f is the unknown non-linear individual reward function, and $\boldsymbol{c}^{i,\boldsymbol{s}\to r} \in \{0,1\}^{D_{\boldsymbol{s}}}$, $\boldsymbol{c}^{i,\boldsymbol{a}\to r} \in \{0,1\}^{D_{\boldsymbol{a}}}$ are binary masks (which may be dynamic or static) that indicate which dimensions of $\boldsymbol{s}_t$ and $\boldsymbol{a}_t$ influence r_t^i. In particular, if there is a causal edge from the k-th dimension of $\boldsymbol{s}_t$ to agent j's individual reward r_t^j in $\mathcal{G}$, then $c^{j,\boldsymbol{s}\to r}(k) = 1$. We emphasize again that we assume an additive structure for the team reward ($R_t = \sum_{i=1}^N r_t^i$) to facilitate interpretable and computationally efficient credit assignment. As discussed in Section 3, this assumption typically aligns closely with standard cooperative MARL benchmarks, and importantly, MACCA remains effective even when rewards are inherently non-additive.

Each binary mask $c_t^{i,\,\boldsymbol{s}\to r} \in \{0,1\}^{D_{\boldsymbol{s}}}$ and $c_t^{i,\,\boldsymbol{a}\to r} \in \{0,1\}^{D_{\boldsymbol{a}}}$ serves two purposes: (1) it reveals the *causal parents* of agent i's individual reward, granting interpretability; and (2) it regularizes ψ_r so that, in an offline dataset with mixed behavior policies, ψ_r does not latch onto spurious correlations among irrelevant state–action dimensions. Without these masks, one would need to predict $\hat{r}_t^i \;=\; \psi_r(s_{1:N,t},\, a_{1:N,t},\, i)$ over all $D_{\boldsymbol{s}} + D_{\boldsymbol{a}}$ dimensions—making it impossible to recover "which features matter" or to prove identifiability. The masks enable both sparsity and a clear DAG structure.

Proposition 4.1 (Identifiability of Causal Structure and Individual Reward Function)**.** *Suppose the joint state $\boldsymbol{s}_t$, joint action $\boldsymbol{a}_t$, team reward R_t are observable while the individual r_t^i for each agent are unobserved, and they are from the Dec-POMDP, as described in Eq 2. Then under the Markov condition and faithfulness assumption (refer to Appendix C), given the current time step's team reward R_t, all the masks $\boldsymbol{c}^{i,\boldsymbol{s}\to r}$, $\boldsymbol{c}^{i,\boldsymbol{a}\to r}$, as well as the function f are identifiable.*

The proposition 4.1 demonstrates that we can identify causal representations from the joint action and state, which serve as the causal parents of the individual reward function we want to fit. This allows us to determine which agent should be responsible for which dimension and thus generate the corresponding individual reward function for each agent. The objective for each agent changes to maximize the sum of individual rewards over an infinite horizon. The proof is in Appendix D.

4.2 Causal Model Learning

In this section, we delve into identifying the unknown causal structure and reward function within the graph $\mathcal{G}$. This is achieved using the causal structure predictor ψ_g, and the individual reward predictor ψ_r. The set $\psi_g = \{\psi_g^{\boldsymbol{s}\to r}, \psi_g^{\boldsymbol{a}\to r}\}$ is to learn the causal structure. Specifically, $\psi_g^{\boldsymbol{s}\to r}$ and $\psi_g^{\boldsymbol{a}\to r}$ are employed to predict the presence of edges in the masks described by Eq 2. We have

$$\hat{\boldsymbol{c}}_t^{i,\boldsymbol{s}\to r} = \psi_g^{\boldsymbol{s}\to r}(\boldsymbol{s}_t, \boldsymbol{a}_t, i), \hat{\boldsymbol{c}}_t^{i,\boldsymbol{a}\to r} = \psi_g^{\boldsymbol{a}\to r}(\boldsymbol{s}_t, \boldsymbol{a}_t, i), \tag{3}$$

where, $\hat{\boldsymbol{c}}_t^{i,\boldsymbol{s}\to r}$ and $\hat{\boldsymbol{c}}_t^{i,\boldsymbol{a}\to r}$ are the predicted masks for agent i at timestep t. Note that these causal masks are time-invariant and can change with state and action. We generate masks at each time step since we consider the inherent complexity of the multi-agent scenario, which has high dimensionality and the dynamic nature of the causal relationships that can evolve over time. Thus, we adopt $\psi_g^{\boldsymbol{s}\to r}$ and $\psi_g^{\boldsymbol{a}\to r}$ to generate mask estimation at each time step t, within the joint state and joint action and agent id as the input. This dynamic mask adaptation facilitates more accurate causal modelling. To further validate this estimation, we have conducted ablation experiments at Section 5.3.

The ψ_r is used for approximating the function f, and is constructed by stacked fully-connection layers. To recover the underlying generative process, i.e., to optimize ψ_r, we minimize the following objective:

$$L_{\mathrm{m}} = \mathbb{E}_{\mathcal{D}}[R_t - \sum_{i=1}^{N} \psi_r(\hat{\boldsymbol{c}}_t^{i,\boldsymbol{s}\to r}, \hat{\boldsymbol{c}}_t^{i,\boldsymbol{a}\to r}, \boldsymbol{s}_t, \boldsymbol{a}_t, i)]^2 + L_{\mathrm{reg}}. \tag{4}$$

The L_{reg} serves as an L1 regularization, akin to the purpose delineated in (Zhang & Spirtes, 2011). Its primary objective is to clear redundant features during training, reduce the number of features that a given depends on, and use the coefficients of other features completely set to zero, which fosters model interpretability and mitigates the risk of overfitting. And it defines as:

$$L_{\mathrm{reg}} = \lambda_1 \textstyle\sum_{i=1}^{N} \|\hat{\boldsymbol{c}}_t^{i,\boldsymbol{s}\to r}\|_1 + \lambda_2 \sum_{i=1}^{N} \|\hat{\boldsymbol{c}}_t^{i,\boldsymbol{a}\to r}\|_1, \tag{5}$$

where $\lambda_{(\cdot)}$ are hyper-parameters. For more details, please refer to Appendix F.

4.3 Policy Learning with Assigned Individual Rewards.

For policy learning, we use the redistributed individual rewards $\tilde{r}_t^i$ to replace the observed team reward R_t. Then, we carry out the policy optimizing over the offline dataset $\mathcal{D}$.

Individual Rewards Assignment. We first assign individual rewards for each agent's state-action-id tuple $\langle \boldsymbol{s}_t, \boldsymbol{a}_t, i\rangle$ in the samples used for policy learning. During such an inference phase of individual rewards predictor, we first utilize a hyperparameter, h, as an element-wise threshold to determine the existence of the inference phase. Elements within the mask $\hat{\boldsymbol{c}}_t^{i,\boldsymbol{s}\to r}$ and $\hat{\boldsymbol{c}}_t^{i,\boldsymbol{a}\to r}$ will be set to 0 if their absolute value is less than h, and 1 otherwise. Then, we assign an individual reward for each agent as,

$$\hat{r}_t^i = \psi_r(\boldsymbol{s}_t, \boldsymbol{a}_t, \hat{\boldsymbol{c}}_t^{i,\boldsymbol{s}\to r}, \hat{\boldsymbol{c}}_t^{i,\boldsymbol{a}\to r}, i). \tag{6}$$

Offline Policy Learning. The process of individual reward assignment is flexible and is able to be inserted into any policy training algorithm. We now describe three practical offline MARL methods, MACCA-CQL, MACCA-OMAR and MACCA-ICQ. In all those methods, they use Q-Value to guide policy learning, for each agent who estimates the $Q^i(o^i, a^i) = E_\pi[\sum_{t=0}^{\infty} \gamma^t R_t]$ with the Bellman backup operator, we then replace the team reward by learned individual reward $\hat{r}_t^i$ as $\hat{Q}^i(o^i, a^i) = E_\pi[\sum_{t=0}^{\infty} \gamma^t \hat{r}_t^i]$, then in the policy improvement step, MACCA-CQL trains actors by minimizing:

$$J_\pi^{\mathrm{CQL}} = \mathbb{E}_{\mathcal{D}}[(\hat{Q}^i(o^i, a^i) - y^i)^2] + \alpha \mathbb{E}_{\mathcal{D}}[\log \sum_{a^i} \exp(\hat{Q}^i(o^i, a^i)) - \mathbb{E}_{a^i \sim \hat{\pi}_\beta^i}[\hat{Q}^i(o^i, a^i)]], \tag{7}$$

where, $y^i = \hat{r}_t^i + \gamma \min_{k=1,2} \bar{Q}^{i,k}(o^{i'}, \bar{\pi}^i(o^{i'}))$ from Fujimoto et al. (2018) to minimize the temporal difference error, $\bar{Q}^i$ represents the target $\hat{Q}$ for the agent i, α is the regularization coefficient, $\hat{\pi}_{\beta^i}$ is the empirical behavior policy of agent i in the dataset. Similarly, MACCA-OMAR updates actors by minimizing:

$$J_\pi^{\mathrm{OMAR}} = -\mathbb{E}_{\mathcal{D}}[(1-\tau)\hat{Q}^i(o^i, \pi^i(o^i)) - \tau(\pi^i(o^i) - \hat{a}_i)^2], \tag{8}$$

where $\hat{a}_i$ is the action provided by the zeroth-order optimizer and $\tau \in [0, 1]$ denotes the coefficient. For the MACCA-ICQ, it updates actors by minimizing:

$$J_\pi^{\mathrm{ICQ}} = \mathbb{E}_{\mathcal{D}}[L_2^\tau(\hat{r}(s, a) + \gamma \bar{Q}^i(o^{i'}, a^{i'}) - \hat{Q}^i(o^i, a^i))], \tag{9}$$

where L_2^τ is the squared loss based on expectile regression and the γ is the discount factor, which determines the present value of future rewards. As MACCA uses individual reward to replace the team reward, we do not directly decompose value function, unlike the prior offline MARL methods (Foerster et al., 2018; Wang et al., 2020; 2022a), thus we do not require fitting an additional advantage value or Q-value estimator, simplifying our method.

Table 1: Average Normalized Score of MPE task with Team Reward

	I-CQL	OMAR	MA-ICQ	MACCA-CQL	MACCA-OMAR	MACCA-ICQ
Exp(CN)	33.6 ± 22.9	44.7 ± 46.6	45.0 ± 23.1	85.4 ± 8.1	**111.7 ± 4.3**	90.4 ± 5.1
Exp(PP)	63.4 ± 38.6	99.9 ± 14.2	87.0 ± 12.3	94.9 ± 27.9	111.0 ± 21.5	**114.4 ± 25.1**
Exp(WORLD)	54.4 ± 17.3	98.7 ± 18.7	43.2 ± 15.7	89.3 ± 14.8	**107.4 ± 11.0**	93.2 ± 12.0
Med(CN)	19.7 ± 8.7	49.6 ± 14.9	30.8 ± 7.3	45.0 ± 8.8	67.9 ± 16.9	**70.3± 10.4**
Med(PP)	50.0 ± 15.6	57.4 ± 13.9	59.4 ± 11.1	61.1 ± 27.1	**87.1 ± 12.2**	77.4 ± 10.5
Med(WORLD)	25.7 ± 21.3	33.4 ± 12.8	35.6 ± 6.0	54.7 ± 11.0	**63.6 ± 8.7**	55.1 ± 3.5
Med-R(CN)	10.8 ± 7.7	26.8 ± 15.2	22.4 ± 9.3	15.9 ± 11.2	**33.2 ± 12.6**	28.6 ± 5.6
Med-R(PP)	18.3 ± 9.5	56.3 ± 16.6	44.2 ± 4.5	32.5 ± 15.1	**69.0 ± 19.3**	64.3 ± 7.8
Med-R(WORLD)	4.5 ± 10.1	28.9 ± 17.2	10.7 ± 2.8	34.8 ± 16.7	**50.9 ± 14.2**	39.9 ± 13.4
Rand(CN)	12.4 ± 9.1	22.9 ± 10.4	6.0 ± 3.1	22.2 ± 4.6	**32.8 ± 9.5**	28.13 ± 4.6
Rand(PP)	5.5 ± 2.8	12.0 ± 5.2	15.6 ± 3.4	14.7 ± 6.7	20.9 ± 8.3	**30.3 ± 5.4**
Rand(WORLD)	0.1 ± 4.5	6.2 ± 6.7	0.6 ± 2.4	8.7 ± 3.3	**15.8 ± 6.1**	10.1 ± 6.6

5 Experiments

Based on the above, our methods include **MACCA-OMAR**, **MACCA-CQL** and **MACCA-ICQ**. For baselines, we compare with both CTDE and independent learning paradigm methods, including **I-CQL** (Kumar et al., 2020): conservative Q-learning in independent paradigm, **OMAR** (Pan et al., 2022): based on I-CQL, but learning better coordination actions among agents using zeroth-order optimization, **MA-ICQ** (Yang et al., 2021): Implicit constraint Q-learning within CTDE paradigm, **SHAQ** (Wang et al., 2022a) and **SQDDPG** (Wang et al., 2020): variants of credit assignment method using Shapley value, which are the SOTA on the online multi-agent RL, **SHAQ-CQL**: In pursuit of a more fair comparison, we integrated CQL with SHAQ, which adopts the architectural framework of SHAQ while using CQL in the estimations of agents' Q-values and the target Q-values, **QMIX-CQL**: conservative Q-learning within CTDE paradigm, following QMIX structure to calculate the Q^{tot} using a mixing layer, which is similar to the MA-ICQ framework. We evaluate those performance in two environments: Multi-agent Particle Environments (MPE) (Lowe et al., 2017) and StarCraft Micromanagement Challenges (SMAC) (Samvelyan et al., 2019). Through these comparative evaluations, we want to highlight the relative effectiveness and superiority of the MACCA approach. Furthermore, we conduct three ablations to investigate the interpretability and efficiency of our method. For detailed information about the environments, please refer to Appendix E.

5.1 General Implementation

Offline Dataset. Following the approach outlined in Justin et al. (2020) and Pan et al. (2022), we classify the offline datasets in all environments into four types: Random, generated by random initialization. Medium-Reply, collected from the replay buffer until the policy reaches medium performance. Medium and Expert, collected from partially trained to moderately performing policies and fully trained policies, respectively. The difference between our setup and Pan et al. (2022) is that we hide individual rewards during training and store the sum of these individual rewards in the dataset as the team reward. By creating these different datasets, we aim to explore how different data qualities affect algorithms. For MPE, we adopt the normalized score as a metric to assess performance. The normalized score is calculated by $100 \times (S - S_{\text{random}})/(S_{\text{expert}} - S_{\text{random}})$ following by Justin et al. (2020), where the $S, S_{\text{random}}, S_{\text{expert}}$ are the evaluation return from the current policy, random set behaviour policy, expert set behaviour policy respectively.

5.2 Main Results

Multi-agent Particle Environment (MPE). We evaluate our method in three distinct environments: Cooperative Navigation (**CN**), Prey-and-Predator (**PP**), and Simple-World (**WORLD**). In the CN environment, three agents aim to reach targets. Observations include position, velocity, and displacements to targets and other agents. Actions are continuous in x and y. Rewards are based on distance to targets, with collision penalties. In the PP environment, three predators chase a random prey. Their state includes position, velocity, and relative displacements. Rewards are based on distance to the prey, with bonuses for captures. The WORLD environment has four allies chasing two faster adversaries. As depicted in Table 1, It can be seen that the algorithms based on MACCA perform better than their respective backbones.

Table 2: Averaged win rate of MACCA-based algorithms and baselines in StarCraft II tasks

Map	Dataset	I-CQL	OMAR	MA-ICQ	MACCA-CQL	MACCA-OMAR	MACCA-ICQ
2s3z (Easy)	Expert	0.70±0.09	0.86±0.08	0.80±0.01	0.88±0.07	**0.99±0.05**	0.95±0.01
	Medium	0.20±0.03	0.17±0.01	0.16±0.07	0.27±0.02	**0.55±0.03**	0.51±0.03
	Medium-Replay	0.11±0.07	0.35±0.08	0.31±0.04	0.25±0.03	0.53±0.01	**0.59±0.04**
5m_vs_6m (Hard)	Expert	0.02±0.02	0.44±0.04	0.38±0.05	0.63±0.02	0.73±0.04	**0.88±0.01**
	Medium	0.01±0.00	0.14±0.02	0.11±0.04	0.19±0.01	**0.20±0.04**	0.15±0.02
	Medium-Replay	0.12±0.01	0.09±0.04	0.18±0.04	0.15±0.02	0.14±0.01	**0.28±0.01**
6h_vs_8z (Super Hard)	Expert	0.00±0.00	0.18±0.08	0.04±0.01	0.59±0.01	**0.75±0.07**	0.60±0.03
	Medium	0.01±0.01	0.12±0.06	0.01±0.01	0.17±0.00	0.20±0.02	**0.22±0.04**
	Medium-Replay	0.03±0.02	0.01±0.01	0.07±0.04	0.14±0.02	0.22±0.01	**0.25±0.05**
MMM2 (Super Hard)	Expert	0.08±0.03	0.10±0.01	0.11±0.01	0.60±0.01	0.69±0.01	**0.71±0.03**
	Medium	0.02±0.01	0.12±0.02	0.08±0.04	0.25±0.07	0.50±0.06	**0.59±0.04**

Table 3: Compare with online off-policy credit assignment baselines in SMAC

Map	Dataset	SHAQ	SQDDPG	SHAQ-CQL	QMIX-CQL	I-CQL	MACCA-CQL
2s3z	Expert	0.10±0.03	0.05±0.01	0.79±0.03	0.73±0.02	0.70±0.09	**0.88±0.07**
	Medium	0.05±0.03	0.07±0.01	0.24±0.01	0.22±0.03	0.20±0.03	**0.27±0.02**
5m_vs_6m	Expert	0.02±0.01	0.00±0.00	0.10±0.03	0.03±0.01	0.02±0.02	**0.63±0.02**
	Medium	0.00±0.00	0.00±0.00	0.06±0.01	0.01±0.01	0.01±0.00	**0.19±0.01**
6h_vs_8z	Expert	0.00±0.00	0.00±0.00	0.02±0.01	0.00±0.00	0.00±0.00	**0.59±0.01**
	Medium	0.00±0.00	0.00±0.00	0.04±0.02	0.00±0.00	0.01±0.01	**0.17±0.00**

StarCraft Micromanagement Challenges (SMAC). In order to show the performance in the scale scene, we specially selected maps with a large number of agents. To illustrate, the map $2s3z$ needs to control 5 agents, including 2 Stalkers and 3 Zealots, the map 6h_vs_8z needs to control 6 Hydralisks against 8 Zealots, and map MMM2 have 1 Medivac, 2 Marauders and 7 Marines. All experiments will run 3 random seeds and the win rate was recorded, and the corresponding standard was calculated. Table 2 shows the result. For most of the tasks, the MACCA-based method shows state-of-the-art performance compared to their baseline algorithms.

Also, we considered testing online off-policy algorithms in the offline setting. To this end, we introduced several baselines in SMAC for comparison with MACCA, as shown in Table 3. The table below shows the results of the added baselines compared to SMAC tasks. It becomes apparent that when directly applied to the offline setting, online off-policy credit assignment algorithms consistently yield suboptimal performance. Our empirical findings underscore that while SHAQ-CQL indeed exhibits advancements QMIX-CQL, our MACCA-CQL clinches the SOTA performance across all tasks.

5.3 Ablation Studies

The Impact of Learned Causal Structure. We varied the value of λ_1 in Eq 5 to control the density of the learned causal structure. Table 4 presents the average cumulative reward and the density of the causal structure during the training process in the MPE-CN environment. The density of the causal structure $\hat{\boldsymbol{c}}_t^{i,\boldsymbol{s}\to r}$, is calculated as $\rho_{sr} = \sum_{i=1}^{N} \frac{1}{d_s^i} \sum_{k=1}^{d_s^i} \boldsymbol{s}_k^{i,\boldsymbol{s}\to r}$, where $\boldsymbol{s}_k^{i,\boldsymbol{s}\to r}$ represent is the value bigger than the threshold h. The results indicate that as λ_1 increases from 0 to 0.5, the causal structure becomes more sparse (ρ_{sr} decreases), resulting in less policy improvement. This can be attributed to the fact that MACCA may not have enough states to predict individual rewards, leading to misguided policy learning accurately. Conversely, setting a relatively low λ_1 may result in a denser structure that incorporates redundant dimensions, hindering policy learning. Therefore, achieving a reasonable causal structure for the reward function can improve both the convergence speed and the performance of policy training. We also provide the ablation for λ_2, please refer to Appendix.F.4.

Table 5: Average normalized scores for ground truth individual reward comparison in MPE-CN

	OMAR	MACCA-OMAR
With GT	114.9 ± 2.4	113.7 ± 2.3
Without GT	43.7 ± 46.6	111.7 ± 4.3

Ground Truth Individual Reward. In the MPE CN expert dataset, we investigate the influence of ground truth individual rewards on agent policy updates. Two scenarios are compared: agents update policies using ground truth individual rewards (GT), and agents primarily rely on team rewards (without GT). Notably, OMAR with GT directly employs individual rewards for policy updates, while MACCA-OMAR with

Table 4: The mean and the standard variance of average normalized score, density rate ρ_{sr} of $\hat{\boldsymbol{c}}_t^{i,\boldsymbol{s}\to r}$ with diverse λ_1 at different time step t in MPE-CN.

λ_1 / t	$1e4$	$3e4$	$5e4$	$1e5$	$2e5$
0	-2.43 ± 8.01(0.98)	-14.87± 7.71(0.90)	-12.356± 5.83(0.81)	9.842± 18.89(0.77)	69.04 ± 19.69(0.72)
0.007	-7.88±5.36(0.94)	**13.26±27.14(0.47)**	**60.18±26.14(0.28)**	**99.78± 19.50(0.15)**	**111.65± 4.28(0.13)**
0.05	-3.66±12.14(0.90)	3.93±42.06(0.34)	10.04± 45.97(0.17)	23.61± 44.18(0.11)	75.81± 34.48(0.10)
0.5	-12.20±3.87(0.87)	-16.19±5.53(0.24)	-8.84± 7.16(0.11)	16.40± 21.04(0.07)	59.23± 35.29(0.01)

GT utilizes individual rewards as a supervisory signal, replacing team rewards in Eq 4. The results, presented in Table 5, the small gap between MACCA+GT and OMAR+GT arises from the extra regularization introduced by jointly learning ψ_g and ψ_r, a design choice that in fact improves generalization when ground truth r_t^i are unavailable. Thus, even though OMAR with GT slightly outperforms MACCA–OMAR when GT is provided, MACCA–OMAR's ability to learn $\hat{r}_t^i$ without supervision is what enables major performance gains over baselines that rely solely on team rewards. For further details on prediction accuracy convergence versus GT, see Appendix F.6

Table 6: Average win rate in SMAC 5m_vs_6m map, expert dataset.

	Win Rate
MACCA (Fully Connected Graph)	0.38 ± 0.02
MACCA (Fixed Graph)	0.50 ± 0.01
MACCA (w.o h clipping)	0.66 ± 0.01
MACCA (w. h clipping)	**0.73 ± 0.04**

The Impact of Causal Graph Types. To investigate the performance under different graph types, we consider three settings. The Fully Connected Graph assumes all variables are causally connected, while The Fixed Graph learns a static graph that is invariant to time by averaging the predicted masks $\hat{c}_t^{i,\cdot\to r}$ overall time steps during training. Our proposed graph setting, as described in Equation 3, learns a graph that depends on the current state s_t and action a_t. Table 6 presents the results of MACCA-OMAR under these different graph types. The Fully Connected Graph yields suboptimal performance due to its inability to differentiate individual agent contributions. The Fixed Graph shows marginal improvement over the Fully Connected Graph but remains limited in capturing the complex dynamic multi-agent causal relationships that vary with time. In contrast, our proposed dynamic graph setting achieves the highest performance by incorporating time-varying information. Additionally, we compared the performance of our method with and without h clipping, where the threshold h filters the causal mask. The results demonstrate that our method with h clipping outperforms the variant without it. This aligns with established practices in earlier works on DAG structural learning (Zheng et al., 2018; Ng et al., 2020), which show the importance of clipping to ensure edge weights converge to zero when working with finite datasets. Appendix F.5 provides additional results of MACCA under different levels of h.

Visualization of Causal Structure. In Figure 3, we provide visualizations of two significant causal structures within the CN environment of MPE. To observe the causal structure learning process more easily, we initialize the $\hat{c}_t^{i,s\to r}$ as a normalized random number close to 1 and the $\hat{c}_t^{i,a\to r}$ close to 0. Over time, we notice that the causal structure $\hat{c}_t^{i,s\to r}$ shifts its focus from considering all dimensions of the agent state to primarily emphasizing the 4th to 10th dimensions of each agent. In this environment, the agent's state comprises 18 dimensions. Specifically, dimensions 0th to 4th us agent's velocity and position, 5th to 9th capture the distance between the agent and three distinct landmarks, 10th to 13th reflect the distances between the agent and other agents, and dimensions 14th to 17th are related to communication, although not applicable in this experiment and thus considered irrelevant. In other words, the dimensions 4th to 9th and 10th to 13th are intuitively linked to individual rewards, aligning with the convergence direction of MACCA. With regard to the causal structure $\hat{c}_t^{i,a\to r}$, as each agent's actions involve continuous motion without extraneous variables, it converges to relevant states that contribute to individual credits for the team reward. The results support the interpretability of relationships between variables through the causal structure.

Table 7: The win rate and loss of different training paradigms by using MACCA-OMAR in SMAC 5m_vs_6m, expert dataset

	Win Rate	Causal Model Loss
TCB	0.62 ± 0.08	0.80 ± 0.02
TCPA	0.73 ± 0.04	0.81 ± 0.01

Training paradigms In MACCA, we train the causal model and policy alternately rather than train the causal model at the beginning. The benefit of alternated training is that the reward model is less accurate at the early stage of training, which encourages agents to extract diverse behaviours that go beyond the dataset. Similar to (Hu et al., 2024), they discuss the usefulness of random rewards prior. We conducted experiments as detailed in Table 7. Here, the **TCB** stands for training the causal model at the

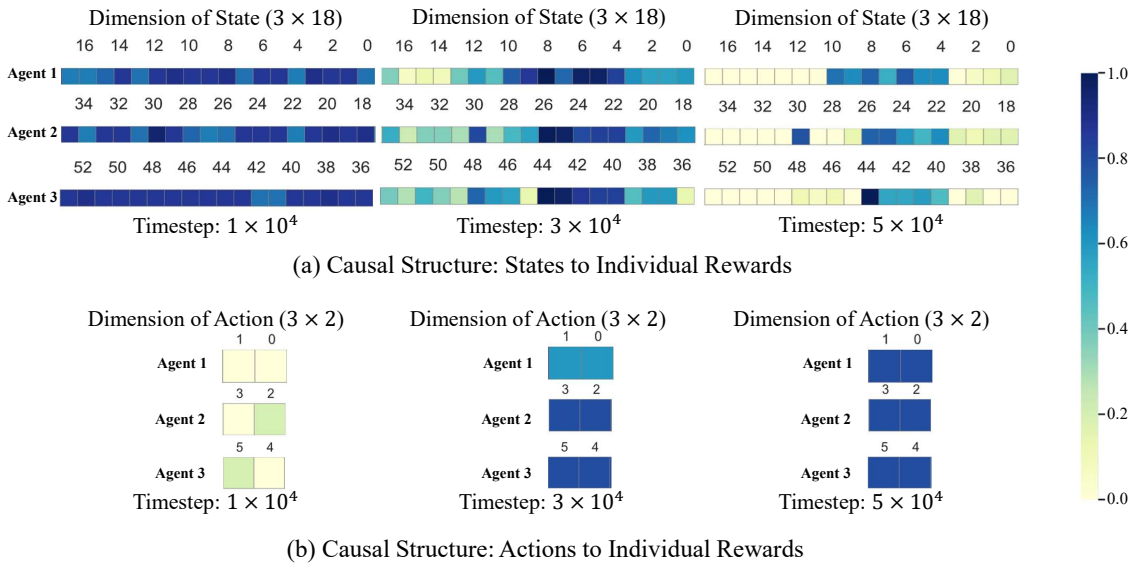

Figure 3: The figure visualizes the causal structure, showing the probability of causal edges from blue (high probability) to yellow (low probability). **(a)** represents the causal structure $\hat{c}_t^{i,\boldsymbol{s}\to r}$ between the state of all agents (18 dimensions for each agent, 54 dimensions for joint state) and the individual reward (1 dimension for each agent). **(b)** represents the causal structure $\hat{c}_t^{i,\boldsymbol{a}\to r}$ between the action of each agent (2 dimensions for each agent, six dimensions for joint action) and the individual reward (1 dimension for each agent).

beginning, and the **TCPA** is training the causal model and policy alternately. The causal model is initially trained with the same training time steps as the alternating setting, which is 10 million steps. According to the result, for both paradigms, the reward model loss converged to comparable levels, and TCPA showed a clear improvement in the win rate.

Robustness to Non-Additive Rewards. On a sparse-reward variant of MPE-CN—where $R_t = 1$ only if all three agents cover distinct landmarks and $R_t = 0$ otherwise (so $\sum_i r_t^i \neq R_t$)—MACCA still outperforms the baseline (Table 8), demonstrating that it can learn meaningful latent individual rewards and effective policies even when the team reward is not decomposable.

Table 8: Performance on the sparse-reward variant of MPE-CN. Despite the highly non-additive team reward, MACCA significantly improves credit assignment and overall policy performance.

Method	Avg. Episode Reward
OMAR	0.18 ± 0.07
MACCA-OMAR	0.42 ± 0.13

6 Conclusion

In conclusion, MACCA emerges as a valuable solution to the credit assignment problem in offline Multi-agent Reinforcement Learning (MARL), providing an interpretable and modular framework for capturing the intricate interactions within multi-agent systems. By leveraging the inherent causal structure of the system, MACCA allows us to disentangle and identify the specific credits of individual agents to team rewards. This enables us to accurately assign credit and update policies accordingly, leading to enhanced performance compared to different baseline methods. The MACCA framework empowers researchers and practitioners to gain deeper insights into the dynamics of multi-agent systems, facilitating the understanding of the causal factors that drive cooperative behavior and ultimately advancing the capabilities of MARL in a variety of real-world applications.

Limitation and Future Work. One limitation of the current work is that the experiments focused on simulated environments rather than real-world scenarios. While the MPE and SMAC environments provide controlled testbeds to evaluate the approach, the performance of MACCA in practical multi-agent applications remains to be investigated. Future work could explore integrating the method with real robot systems or testing it on datasets collected from real-world multi-agent interactions to further validate its practicality and robustness.

Acknowledge

This work was supported by the Engineering and Physical Sciences Research Council [grant number EP/Y003187/1]

References

Rishabh Agarwal, Dale Schuurmans, and Mohammad Norouzi. An optimistic perspective on offline reinforcement learning. In *International Conference on Machine Learning*, pp. 104–114. PMLR, 2020.

Yu-han Chang, Tracey Ho, and Leslie Kaelbling. All learning is local: Multi-agent learning in global reward games. In *Advances in Neural Information Processing Systems*, volume 16. MIT Press, 2003.

Sirui Chen, Zhaowei Zhang, Yali Du, and Yaodong Yang. Stas: Spatial-temporal return decomposition for multi-agent reinforcement learning. In *In Proceedings of the AAAI conference on artificial intelligence*, 2023.

Christian Schroeder de Witt, Tarun Gupta, Denys Makoviichuk, Viktor Makoviychuk, Philip HS Torr, Mingfei Sun, and Shimon Whiteson. Is independent learning all you need in the starcraft multi-agent challenge? *arXiv preprint arXiv:2011.09533*, 2020.

Yali Du, Lei Han, Meng Fang, Ji Liu, Tianhong Dai, and Dacheng Tao. Liir: Learning individual intrinsic reward in multi-agent reinforcement learning. In *Advances in Neural Information Processing Systems*, volume 32. Curran Associates, Inc., 2019.

Yali Du, Joel Z Leibo, Usman Islam, Richard Willis, and Peter Sunehag. A review of cooperation in multi-agent learning. *arXiv preprint arXiv:2312.05162*, 2023.

Fan Feng, Biwei Huang, Kun Zhang, and Sara Magliacane. Factored adaptation for non-stationary reinforcement learning. In *Advances in Neural Information Processing Systems*, volume 35, pp. 31957–31971. Curran Associates, Inc., 2022.

Jakob Foerster, Gregory Farquhar, Triantafyllos Afouras, Nantas Nardelli, and Shimon Whiteson. Counterfactual multi-agent policy gradients. In *Proceedings of the AAAI conference on artificial intelligence*, volume 32, 2018.

Scott Fujimoto, Herke Hoof, and David Meger. Addressing function approximation error in actor-critic methods. In *International Conference on Machine Learning*, pp. 1587–1596. PMLR, 2018.

St John Grimbly, Jonathan Shock, and Arnu Pretorius. Causal multi-agent reinforcement learning: Review and open problems. In *Cooperative AI Workshop, Advances in Neural Information Processing Systems*, 2021.

Lewis Hammond, James Fox, Tom Everitt, Ryan Carey, Alessandro Abate, and Michael Wooldridge. Reasoning about causality in games. *Artificial Intelligence*, 320:103919, 2023. ISSN 0004-3702. doi: https://doi.org/10.1016/j.artint.2023.103919.

Hao Hu, Yiqin Yang, Jianing Ye, Ziqing Mai, and Chongjie Zhang. Unsupervised behavior extraction via random intent priors. *Advances in Neural Information Processing Systems*, 36, 2024.

Jiaheng Hu, Peter Stone, and Roberto Martín-Martín. Causal policy gradient for whole-body mobile manipulation. In *Robotics: Science and Systems XIX*, 2023.

Biwei Huang, Fan Feng, Chaochao Lu, Sara Magliacane, and Kun Zhang. Adarl: What, where, and how to adapt in transfer reinforcement learning. In *International Conference on Learning Representations*, 2021.

Biwei Huang, Chaochao Lu, Liu Leqi, José Miguel Hernández-Lobato, Clark Glymour, Bernhard Schölkopf, and Kun Zhang. Action-sufficient state representation learning for control with structural constraints. In *International Conference on Machine Learning*, pp. 9260–9279. PMLR, 2022.

Natasha Jaques, Angeliki Lazaridou, Edward Hughes, Caglar Gulcehre, Pedro Ortega, DJ Strouse, Joel Z Leibo, and Nando De Freitas. Social influence as intrinsic motivation for multi-agent deep reinforcement learning. In *International Conference on Machine Learning*, pp. 3040–3049. PMLR, 2019.

Jiechuan Jiang and Zongqing Lu. Offline decentralized multi-agent reinforcement learning. *arXiv preprint arXiv:2108.01832*, 2021.

Fu Justin, Kumar Aviral, Nachum Ofir, Tucker George, and Levine Sergey. D4rl: Datasets for deep data-driven reinforcement learning. *arXiv preprint arXiv:2004.07219*, 2020.

Ilya Kostrikov, Ashvin Nair, and Sergey Levine. Offline reinforcement learning with implicit q-learning. In *International Conference on Learning Representations*, 2022.

Aviral Kumar, Aurick Zhou, George Tucker, and Sergey Levine. Conservative q-learning for offline reinforcement learning. In *Advances in Neural Information Processing Systems*, volume 33, pp. 1179–1191. Curran Associates, Inc., 2020.

Sergey Levine, Aviral Kumar, George Tucker, and Justin Fu. Offline reinforcement learning: Tutorial, review, and perspectives on open problems. *arXiv preprint arXiv:2005.01643*, 2020.

Jiahui Li, Kun Kuang, Baoxiang Wang, Furui Liu, Long Chen, Fei Wu, and Jun Xiao. Shapley counterfactual credits for multi-agent reinforcement learning. In *Proceedings of the 27th ACM SIGKDD Conference on Knowledge Discovery & Data Mining*, pp. 934–942, 2021.

Ryan Lowe, Yi Wu, Aviv Tamar, Jean Harb, Pieter Abbeel, and Igor Mordatch. Multi-agent actor-critic for mixed cooperative-competitive environments. In *Proceedings of the 31st International Conference on Neural Information Processing Systems*, pp. 6382–6393, 2017.

Xueguang Lyu, Yuchen Xiao, Brett Daley, and Christopher Amato. Contrasting centralized and decentralized critics in multi-agent reinforcement learning. *In Proceedings of the 20th International Conference on Autonomous Agents and MultiAgent Systems*, 2021.

Kevin Patrick Murphy. *Dynamic bayesian networks: representation, inference and learning*. University of California, Berkeley, 2002.

Ignavier Ng, AmirEmad Ghassami, and Kun Zhang. On the role of sparsity and dag constraints for learning linear dags. In *Advances in Neural Information Processing Systems*, volume 33, pp. 17943–17954. Curran Associates, Inc., 2020.

Frans A Oliehoek, Christopher Amato, et al. *A concise introduction to decentralized POMDPs*, volume 1. Springer, 2016.

Ling Pan, Longbo Huang, Tengyu Ma, and Huazhe Xu. Plan better amid conservatism: Offline multi-agent reinforcement learning with actor rectification. In *International Conference on Machine Learning*, pp. 17221–17237. PMLR, 2022.

Judea Pearl. *Causality: Models, Reasoning and Inference*. Cambridge University Press, 2009a.

Judea Pearl. *Causality*. Cambridge university press, 2009b.

Silviu Pitis, Elliot Creager, Ajay Mandlekar, and Animesh Garg. Mocoda: Model-based counterfactual data augmentation. In *Advances in Neural Information Processing Systems*, volume 35, pp. 18143–18156. Curran Associates, Inc., 2022.

Tabish Rashid, Mikayel Samvelyan, Christian Schroeder De Witt, Gregory Farquhar, Jakob Foerster, and Shimon Whiteson. Monotonic value function factorisation for deep multi-agent reinforcement learning. *The Journal of Machine Learning Research*, 21(1):7234–7284, 2020.

Mikayel Samvelyan, Tabish Rashid, Christian Schroeder De Witt, Gregory Farquhar, Nantas Nardelli, Tim GJ Rudner, Chia-Man Hung, Philip HS Torr, Jakob Foerster, and Shimon Whiteson. The starcraft multi-agent challenge. *arXiv preprint arXiv:1902.04043*, 2019.

Peter Spirtes, Clark N Glymour, Richard Scheines, and David Heckerman. *Causation, prediction, and search*. MIT press, 2000.

Peter Sunehag, Guy Lever, Audrunas Gruslys, Wojciech Marian Czarnecki, Vinicius Zambaldi, Max Jaderberg, Marc Lanctot, Nicolas Sonnerat, Joel Z Leibo, Karl Tuyls, et al. Value-decomposition networks for cooperative multi-agent learning. *In Proceedings of the 17th International Conference on Autonomous Agents and MultiAgent Systems*, 2018.

Wei-Cheng Tseng, Tsun-Hsuan Johnson Wang, Yen-Chen Lin, and Phillip Isola. Offline multi-agent reinforcement learning with knowledge distillation. In *Advances in Neural Information Processing Systems*, volume 35, pp. 226–237. Curran Associates, Inc., 2022.

Jianhong Wang, Yuan Zhang, Tae-Kyun Kim, and Yunjie Gu. Shapley q-value: A local reward approach to solve global reward games. In *Proceedings of the AAAI Conference on Artificial Intelligence*, volume 34, pp. 7285–7292, 2020.

Jianhong Wang, Yuan Zhang, Yunjie Gu, and Tae-Kyun Kim. Shaq: Incorporating shapley value theory into multi-agent q-learning. In *Advances in Neural Information Processing Systems*, volume 35, pp. 5941–5954, 2022a.

Mianchu Wang, Rui Yang, Xi Chen, and Meng Fang. Goplan: Goal-conditioned offline reinforcement learning by planning with learned models. In *NeurIPS 2023 Workshop on Goal-Conditioned Reinforcement Learning*, 2023.

Zizhao Wang, Xuesu Xiao, Zifan Xu, Yuke Zhu, and Peter Stone. Causal dynamics learning for task-independent state abstraction. In *International Conference on Machine Learning*, pp. 23151–23180, 2022b.

Christopher KI Williams and Carl Edward Rasmussen. *Gaussian processes for machine learning*, volume 2. MIT press Cambridge, MA, 2006.

Rui Yang, Yiming Lu, Wenzhe Li, Hao Sun, Meng Fang, Yali Du, Xiu Li, Lei Han, and Chongjie Zhang. Rethinking goal-conditioned supervised learning and its connection to offline rl. In *International Conference on Learning Representations*, 2022.

Yiqin Yang, Xiaoteng Ma, Chenghao Li, Zewu Zheng, Qiyuan Zhang, Gao Huang, Jun Yang, and Qianchuan Zhao. Believe what you see: Implicit constraint approach for offline multi-agent reinforcement learning. In *Advances in Neural Information Processing Systems*, volume 34, pp. 10299–10312, 2021.

Tianhe Yu, Garrett Thomas, Lantao Yu, Stefano Ermon, James Y Zou, Sergey Levine, Chelsea Finn, and Tengyu Ma. Mopo: Model-based offline policy optimization. In *Advances in Neural Information Processing Systems*, volume 33, pp. 14129–14142, 2020.

Jiji Zhang and Peter Spirtes. Intervention, determinism, and the causal minimality condition. *Synthese*, 182 (3):335–347, 2011.

Junzhe Zhang and Elias Bareinboim. Markov decision processes with unobserved confounders: A causal approach. Technical report, Technical report, Technical Report R-23, Purdue AI Lab, 2016.

Junzhe Zhang, Daniel Kumor, and Elias Bareinboim. Causal imitation learning with unobserved confounders. In *Advances in Neural Information Processing Systems*, volume 33, pp. 12263–12274, 2020.

Yudi Zhang, Yali Du, Biwei Huang, Ziyan Wang, Jun Wang, Meng Fang, and Mykola Pechenizkiy. Interpretable reward redistribution in reinforcement learning: A causal approach. In *Advances in Neural Information Processing Systems*, 2023.

Xun Zheng, Bryon Aragam, Pradeep K Ravikumar, and Eric P Xing. Dags with no tears: Continuous optimization for structure learning. In *Advances in Neural Information Processing Systems*, volume 31, 2018.

A Broader Impact Statements

The proposed work advances offline multi-agent reinforcement learning by introducing a general approach to credit assignment that can be integrated with existing algorithms, yielding significant performance gains in static-data settings. Beyond academic benchmarks, MACCA's identifiable causal structures offer critical value in real-world applications: for instance, multi-robot coordination in logistics or disaster-response teams—where understanding each robot's contribution is essential for fault diagnosis and task allocation; autonomous driving fleets—where clear, interpretable attributions of responsibility among vehicles improve accountability, safety, and regulatory compliance; and distributed control systems in domains such as smart grids or algorithmic trading—where transparent, causally grounded decisions enhance reliability and risk management. At the same time, we recognize risks inherent in learning causal models from biased or incomplete offline datasets—misestimated causal relations could lead to unfair credit assignment or unsafe behavior in high-stakes environments. To mitigate these risks, we emphasize rigorous dataset auditing to detect sampling biases, validation of learned causal structures through simulation before deployment, and cautious incremental rollout in mission-critical applications to ensure that decisions remain safe and equitable.“‘

B Reproducibility Statements

To promote transparent and accountable research practices, we have prioritized the reproducibility of our method. All experiments conducted in this study adhere to controlled conditions and well-known environments and datasets, with detailed descriptions of the experimental settings available in Section 5 and Appendix E. The implementation specifics for all the baseline methods and our proposed MACCA are thoroughly outlined in Section 4 and Appendix F.

C Markov and Faithfulness Assumptions

A directed acyclic graph (DAG), $\mathcal{G} = (\boldsymbol{V}, \boldsymbol{E})$, can be deployed to represent a graphical criterion carrying out a set of conditions on the paths, where $\boldsymbol{V}$ and $\boldsymbol{E}$ denote the set of nodes and the set of directed edges, separately.

Definition C.1. (d-separation (Pearl, 2009a)). A set of nodes $\boldsymbol{Z} \subseteq \boldsymbol{V}$ blocks the path p if and only if (1) p contains a chain $i \to m \to j$ or a fork $i \leftarrow m \to j$ such that the middle node m is in $\boldsymbol{Z}$, or (2) p contains a collider $i \to m \leftarrow j$ such that the middle node m is not in $\boldsymbol{Z}$ and such that no descendant of m is in $\boldsymbol{Z}$. Let $\boldsymbol{X}$, $\boldsymbol{Y}$ and $\boldsymbol{Z}$ be disjunct sets of nodes. If and only if the set $\boldsymbol{Z}$ blocks all paths from one node in $\boldsymbol{X}$ to one node in $\boldsymbol{Y}$, $\boldsymbol{Z}$ is considered to d-separate $\boldsymbol{X}$ from $\boldsymbol{Y}$, denoting as $(\boldsymbol{X} \perp_d \boldsymbol{Y} \mid \boldsymbol{Z})$.

Definition C.2. (Global Markov Condition (Spirtes et al., 2000; Pearl, 2009a)). If, for any partition $(\boldsymbol{X}, \boldsymbol{Y}, \boldsymbol{Z})$, $\boldsymbol{X}$ is d-separated from $\boldsymbol{Y}$ given $\boldsymbol{Z}$, i.e. $\boldsymbol{X} \perp_d \boldsymbol{Y} \mid \boldsymbol{Z}$. Then the distribution P over $\boldsymbol{V}$ satisfies the global Markov condition on graph G, and can be factorizes as, $P(\boldsymbol{X}, \boldsymbol{Y} \mid \boldsymbol{Z}) = P(\boldsymbol{X} \mid \boldsymbol{Z})P(\boldsymbol{Y} \mid \boldsymbol{Z})$. That is, $\boldsymbol{X}$ is conditionally independent of $\boldsymbol{Y}$ given $\boldsymbol{Z}$, writing as $\boldsymbol{X} \perp\!\!\!\perp \boldsymbol{Y} \mid \boldsymbol{Z}$.

Definition C.3. (Faithfulness Assumption (Spirtes et al., 2000; Pearl, 2009a)). The variables, which are not entailed by the Markov Condition, are not independent of each other.

Under the above assumptions, we can apply d-separation as a criterion to understand the conditional independencies from a given DAG G. That is, for any disjoint subset of nodes $\boldsymbol{X}, \boldsymbol{Y}, \boldsymbol{Z} \subseteq \boldsymbol{V}$, $(\boldsymbol{X} \perp\!\!\!\perp \boldsymbol{Y} \mid \boldsymbol{Z})$ and $\boldsymbol{X} \perp_d \boldsymbol{Y} \mid \boldsymbol{Z}$ are the necessary and sufficient condition of each other.

D Proof of Identifiability

Proposition D.1 (Individual Reward Function Identifiability)**.** *Suppose the joint state $\boldsymbol{s}_t$, joint action $\boldsymbol{a}_t$, team reward R_t are observable while the individual r_t^i for each agent are unobserved, and they are from the Dec-POMDP, as described in Eq 2. Then, under the Markov condition and faithfulness assumption, given the current time step's team reward R_t, all the masks $\boldsymbol{c}^{\boldsymbol{s}\to r,i}$, $\boldsymbol{c}^{\boldsymbol{a}\to r,i}$, as well as the function f are identifiable.*

Assumption We assume that, $\epsilon_{i,t}$ in Eq 2 are i.i.d additive noise. From the weight-space view of Gaussian Process (Williams & Rasmussen, 2006) and equation.6, equivalently, the causal models for r_t^i can be represented as follows,

$$r_t^i = f(\boldsymbol{c}_t^{i,\boldsymbol{s}\to r} \odot \boldsymbol{s}_t, \boldsymbol{c}_t^{i,\boldsymbol{a}\to r} \odot \boldsymbol{a}_t, i) + \epsilon_{r,t} = {W_f}^T \phi_r(\boldsymbol{s}_t, \boldsymbol{a}_t, i) + \epsilon_{i,t} \tag{10}$$

where $\forall i \in [1, N]$, and ϕ_r denote basis function sets.

As $\boldsymbol{s}_t = \{s^1_{1,t}, ..., s^1_{d^1_s,t}, ..., s^N_{1,t}...., s^N_{d^N_s,t}\}$ and $\boldsymbol{a}_t = \{a^1_{1,t}, ..., a^1_{d^1_a,t}, ..., a^N_{1,t}...., a^N_{d^N_a,t}\}$. We denote the variable set in the system by $\boldsymbol{V} = \{\boldsymbol{V}_0, ..., \boldsymbol{V}_T\}$, where $\boldsymbol{V}_t = \boldsymbol{s}_t \cup \boldsymbol{a}_t \cup R_t$, and the variables form a Bayesian network $\mathcal{G}$. Following AdaRL (Huang et al., 2021), there are possible edges only from $\boldsymbol{s}^i_{k,t} \in \boldsymbol{s}_t$ to r^i_t, and from $\boldsymbol{a}^i_{j,t} \in \boldsymbol{a}_t$ to r^i_t in $\mathcal{G}$, where k, j are dimension index in $[1, ..., d^N_s]$ and $[1, ..., d^N_a]$ respectively. In particular, the r^i_t are unobserved, while $R_t = \sum_{i=1}^N r^i_t$ is observed. Thus, there are deterministic edges from each r^i_t to R_t.

Proof of the Proposition B.1 We aim to prove that, given the team reward R_t, and the $\boldsymbol{c}^{i,\boldsymbol{s}\to r}$, $\boldsymbol{c}^{i,\boldsymbol{a}\to r}$ and r^i_t are identifiable. Following the above assumption, we can rewrite the Eq 2 to the following,

$$\begin{aligned} R_t &= \sum_{i=1}^N r^i_t \\ &= \sum_{i=1}^N \left[{W_f}^T \phi_r(\boldsymbol{s}_t, \boldsymbol{a}_t, i) + \epsilon_{i,t} \right] \\ &= {W_f}^T \sum_{i=1}^N \phi_r(\boldsymbol{s}_t, \boldsymbol{a}_t, i) + \sum_{i=1}^N \epsilon_{i,t}. \end{aligned} \tag{11}$$

For simplicity, we replace the components in Eq 11 by,

$$\begin{aligned} \Phi_{r,t} &= \sum_{i=1}^N \phi_r(\boldsymbol{s}_t, \boldsymbol{a}_t, i), \\ \mathcal{E}_{r,t} &= \sum_{i=1}^N \epsilon_{i,t}. \end{aligned} \tag{12}$$

Consequently, we derive the following equation,

$$R_t = {W_f}^T \Phi_{r,t}(X_t) + \mathcal{E}_{r,t}, \tag{13}$$

where $X_t := [\boldsymbol{s}_t, \boldsymbol{a}_t, i]^N_{i=1}$ representing the concatenation of the covariates $\boldsymbol{s}_t$, $\boldsymbol{a}_t$ and i, from $i = 1$ to N.

Then we can obtain a closed-form solution of ${W_f}^T$ in Eq 13 by modelling the dependencies between the covariates X_t and response variables R_t. One classical approach to finding such a solution involves minimizing the quadratic cost and incorporating a weight-decay regularizer to prevent overfitting. Specifically, we define the cost function as,

$$C(W_f) = \frac{1}{2} \sum_{X_t, R_t \sim \mathcal{D}} (R_t - {W_f}^T \Phi_{r,t}(X_t))^2 + \frac{1}{2} \lambda \|W_f\|^2. \tag{14}$$

where X_t and long-term returns R_t, which are sampled from the offline dataset $\mathcal{D}$. λ is the weight-decay regularization parameter. To find the closed-form solution, we differentiate the cost function with respect to W_f and set the derivative to zero:

$$\frac{\partial C(W_f)}{\partial W_f} \to 0. \tag{15}$$

Solving Eq 15 will yield the closed-form solution for W_f, as

$$W_f = (\lambda I_d + \Phi_{r,t} {\Phi_{r,t}}^T)^{-1} \Phi_{r,t} R_t = \Phi_{r,t} ({\Phi_{r,t}}^T \Phi_{r,t} + \lambda I_n)^{-1} R_t. \tag{16}$$

Therefore, W_f, which indicates the causal structure and strength of the edge, can be identified from the observed data. In summary, given team reward R_t, the binary masks, $\boldsymbol{c}^{i,\boldsymbol{s}\to r}$, $\boldsymbol{c}^{i,\boldsymbol{a}\to r}$ and individual r^i_t are identifiable.

Considering the Markov condition and faithfulness assumption, we can conclude that for any pair of variables $V_k, V_j \in \boldsymbol{V}$, V_k and V_j are not adjacent in the causal graph $\mathcal{G}$ if and only if they are conditionally independent given some subset of $\{V_l \mid l \neq k, l \neq j\}$. Additionally, since there are no instantaneous causal relationships and the direction of causality can be determined if an edge exists, the binary structural masks $\boldsymbol{c}^{i,\boldsymbol{s}\to r}$ and $\boldsymbol{c}^{i,\boldsymbol{a}\to r}$ defined over the set $\boldsymbol{V}$ are identifiable with conditional independence relationships (Huang et al., 2022). Consequently, the functions f in Equation 2 are also identifiable.

E Environments Setting

We adopt the open-source implementations for the multi-agent particle environment (Lowe et al., 2017)[1] and SMAC(Samvelyan et al., 2019)[2]. The tasks in the multi-agent particle environments are illustrated in Figures 4(a)-(c). The Cooperative Navigation (CN) task involves 3 agents and 3 landmarks, requiring agents to cooperate in covering the landmarks without collisions. In the Predator-Prey (PP) task, 3 predators collaborate to capture prey that is faster than them. Finally, the WORLD task features 4 slower cooperating agents attempting to catch 2 faster adversaries, with the adversaries aiming to consume food while avoiding capture.

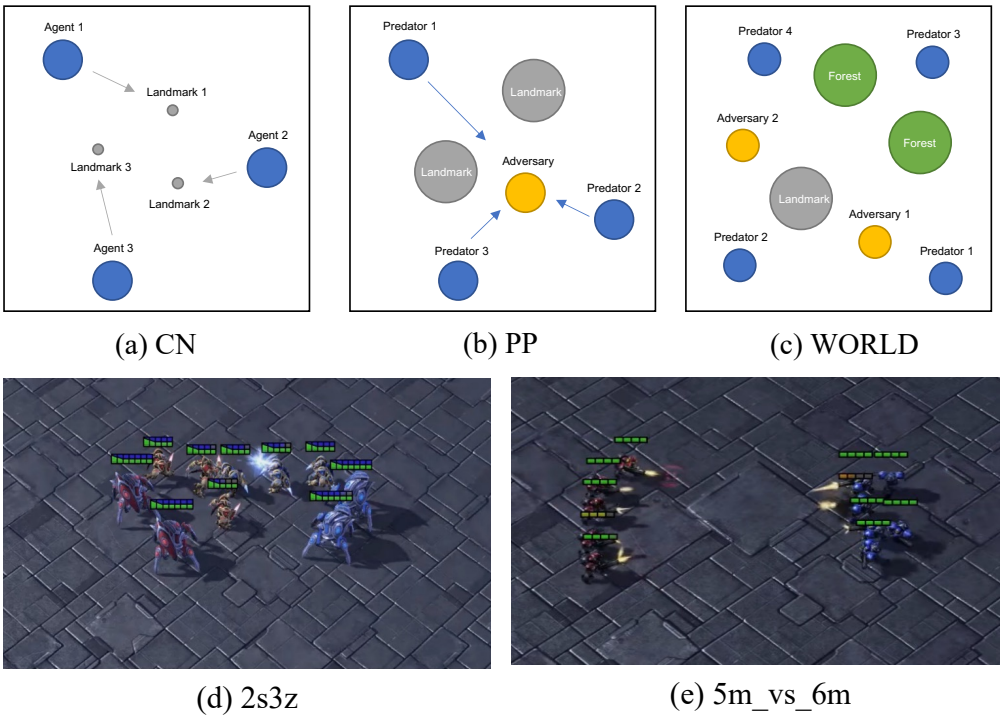

(a) CN (b) PP (c) WORLD

(d) 2s3z (e) 5m_vs_6m

Figure 4: Visualization of different environment in the experiments, **(a)-(c):** Multi-agent Particle Environments (MPE), **(d)-(e):** StarCraft Micromanagement Challenges (SMAC)

Datasets. During training, we utilize the team reward as input, while for evaluation purposes, we compare the performance with the ground truth individual reward. As a result, the expert and random scores for the Cooperative Navigation, Predator-Prey and World tasks are as follows: Cooperative Navigation - expert: 516.526, random: 160.042; Predator-Prey - expert: 90.637, random: -2.569; World - expert: 34.661, random: -8.734;

[1]https://github.com/openai/multiagent-particle-envs
[2]https://github.com/oxwhirl/smac

F Implementations

F.1 Algorithm

Algorithm 1 MACCA: **M**ulti-**A**gent **C**ausal **C**redit **A**ssignment

for training step $t = 1$ to T **do**
  Sample trajectories from $\mathcal{D}$, save in minibatch $\mathcal{B}$
  for agent $i = 1$ to N **do**
    Update the team reward R_t to $\hat{r}_t^i$ in $\mathcal{B}$ (Eq 6)
    Optimize ψ_m: $\psi_m \leftarrow \psi_m - \alpha \nabla_{\psi_m} L_m$ (Eq 4)
  Update policy π with minibatch $\mathcal{B}$ (Eq 7, Eq 8 or Eq 9)
  Reset $\mathcal{B} \leftarrow \emptyset$

F.2 Model Structure

The parametric generative model ψ_{m} used in MACCA consists of two parts: ψ_{g} and ψ_{r}. The function of ψ_{g} is to predict the causal structure, which determines the relationships between the environment variables. The role of ψ_{r} is to generate individual rewards based on the joint state and action information. This prediction is achieved through a network architecture that includes three fully-connected layers with an output size of 256, followed by an output layer with a single output. Each hidden layer is activated using the rectified linear unit (ReLU) activation function.

During the training process, the generative model is optimized to learn the causal structure and generate individual rewards that align with the observed team rewards. The model parameters are updated using Adam, to minimize the discrepancy between the predicted sum of individual rewards and the team rewards. The training process involves iteratively adjusting the parameters to improve the accuracy of the predictions.

For a more detailed overview of the training process, including the specific loss functions and optimization algorithms used, please refer to Figure 2. The Figure provides a step-by-step illustration of the training pipeline, helping to visualize the flow of information and the interactions between different components of the generative model.

Table 9: The Common Hyperparameters.

hyperparameters	value	hyperparameters	value
steps per update	100	optimizer	Adam
batch size	1024	learning rate	3×10^{-4}
hidden layer dim	64	γ	0.95
evaluation interval	1000	evaluation episodes	10

Table 10: Hyperparameters for OMAR, CQL and MACCA

	OMAR τ	CQL α	MACCA λ_1	MACCA λ_2	MACCA r_{lr}	MACCA h
Expert	0.9	5.0	7e-3	7e-3	5e-2	0.1
Medium	0.7	0.5	5e-3	5e-3	5e-2	0.1
Medium-Replay	0.7	1.0	5e-3	7e-3	5e-2	0.1
Random	0.99	1.0	1e-7	1e-3	5e-2	0.1

F.3 Hyper-parameters

The common hyperparameters are shown in Table.9. The neural network used in training is initialized from scratch and optimized using the Adam optimizer with a learning rate of 3×10^{-4}. The policy learning process involves varying initial learning rates based on the specific algorithm, while the hyperparameters for policy learning, including a discount factor of 0.95, are consistent across all tasks.

The training procedure differs across tasks. For MPE, the training duration ranges from 20,000 to 60,000 iterations, with longer training for behavior policies that perform poorly. The number of steps per update is set to 100.

During each training iteration, trajectories are sampled from the offline data, and the generated individual reward is replaced with the team reward for policy updates. The training of ψ_{cau} is performed concurrently with ψ_{rew}. Validation is conducted after each epoch, and the average metrics are computed using 5 random seeds for reliable evaluation.

The hyperparameters specific to training MACCA models can be found in Table 10. All experiments were conducted on a high-performance computing (HPC) system featuring 128 Intel Xeon processors running at 2.2 GHz, 5 TB of memory, and an Nvidia A100 PCIE-40G GPU. This computational setup ensures efficient processing and reliable performance throughout the experiments.

F.4 Ablation for λ_2

We have conducted ablation experiments on λ_2 and show the results in the Table 11.

Table 11: The mean and the standard variance of average normalized score, sparsity rate ρ_{ar} of $\hat{\boldsymbol{c}}_t^{i,\boldsymbol{a}\to r}$ with diverse λ_2 at different time step t in MPE-CN.

λ_2 / t	$1e4$	$5e4$	$1e5$	$2e5$
0	17.4 ± 15.2(0.98)	93.1 ± 6.4 (1.0)	105 ± 3.5 (1.0)	107.7 ± 10.2 (1.0)
0.007	19.9 ± 12.4 (0.8	**90.2 ± 7.1 (1.0)**	**108.8 ± 4.0 (1.0)**	**111.7 ± 4.3(1.0)**
0.5	13.3 ± 11.1 (0.68)	100.5 ± 14.0 (0.84)	102.9 ± 16.4 (0.87)	108.4 ± 6.4 (0.98)
5.0	2.3 ± 9.8 (0.0)	-1.3 ± 25.4 (0.34)	70.4 ± 18.0 (0.62)	100.1 ± 7.4 (0.75)

F.5 Ablation for h

The selection of h can influence the sparsity of the causal graph. h can be selected by parameter sweeping. For simplicity, we use $h = 0.1$ for all tasks in the experiments, which leads to strong performance. we conduct additional experiments under different h in SMAC 5m_vs_6m Medium Dataset with MACCA-OMAR. The results are as follows,

Table 12: The mean and the standard variance of the average normalized score, sparsity rate ρ_{ar} of $\hat{\boldsymbol{c}}_t^{i,\boldsymbol{a}\to r}$ with diverse h in SMAC 5m_vs_6m.

h	Win Rate	ρ_{sr}	ρ_{ar}	Causal Model Loss
0	0.12 ± 0.02	1.0 ± 0.0	1.0 ± 0.0	0.15 ± 0.05
0.01	0.14 ±0.03	0.96 ± 0.12	0.72 ± 0.12	0.07 ± 0.01
0.05	0.16 ±0.02	0.81 ± 0.07	0.66 ± 0.04	0.09 ± 0.04
0.1	0.20 ± 0.04	0.73 ± 0.04	0.54± 0.08	0.05 ± 0.02
0.5	0.17 ± 0.01	0.52 ± 0.10	0.43 ± 0.07	0.12 ± 0.06

The causal graph become more sparse (fewer edges between nodes) with the increase of h. The performance of win rate goes up with the increase of h but decrease after $h > 0.1$, due to potential inclusion of redudance information.

F.6 Prediction Accuracy After Convergence (By Dataset Quality)

After convergence, we measure per-agent errors between redistributed rewards $\hat{r}_t^i$ and true r_t^i. Table 13 shows MSE and MAE (averaged over time and three random seeds) for Expert, Medium, Medium-Replay, and Random datasets.

Table 13: Per-Agent Prediction Errors After Convergence

Dataset Quality	MSE	MAE
Expert	0.12 ± 0.02	0.65 ± 0.10
Medium	0.24 ± 0.05	1.12 ± 0.15
Medium-Replay	0.38 ± 0.08	1.78 ± 0.20
Random	1.60 ± 0.12	4.45 ± 0.30

These results indicate that, once MACCA has converged, the redistributed rewards closely track the true individual rewards in high-quality data (Expert), with an MSE of only 0.12 and MAE of 0.65. As dataset quality degrades—Medium, Medium-Replay, and Random—the errors increase proportionally, reflecting noisier or more random behavior, yet remain within reasonable bounds. Even on the Random dataset, where behavior is least structured, an MAE of 2.45 demonstrates that ψ_r still captures meaningful individual-reward signals after training.

F.7 Computational Resources and Training Times

All experiments were conducted on a heterogeneous computing cluster running Ubuntu Linux. The hardware configuration included a mix of CPU models (Dual Intel Xeon E5-2650, E5-2680 v2, and E5-2690 v3) with a total of 180 CPU cores and 500 GB of system memory. For GPU acceleration, we utilized three NVIDIA A30 GPUs.

The average wall-clock training time (for 10 million environment steps) of each MACCA variant is summarized in Table 14. These timings include both causal model learning and policy optimization under the alternating training scheme; the causal model component accounts for approximately 8–15% of the total time.

Environment	**MACCA Variant**	**Training Time (hrs)**
MPE (CN, PP, WORLD)	MACCA-OMAR	4.2
SMAC (2s3z)	MACCA-OMAR	7.8
SMAC (5m_vs_6m)	MACCA-OMAR	9.5
SMAC (6h_vs_8z)	MACCA-OMAR	11.2
SMAC (MMM2)	MACCA-OMAR	12.0

Table 14: Average wall-clock training time for each MACCA-OMAR run (10 million environment steps).